

Journal of Materials Chemistry A

Accepted Manuscript



This is an *Accepted Manuscript*, which has been through the Royal Society of Chemistry peer review process and has been accepted for publication.

Accepted Manuscripts are published online shortly after acceptance, before technical editing, formatting and proof reading. Using this free service, authors can make their results available to the community, in citable form, before we publish the edited article. We will replace this *Accepted Manuscript* with the edited and formatted *Advance Article* as soon as it is available.

You can find more information about *Accepted Manuscripts* in the [Information for Authors](#).

Please note that technical editing may introduce minor changes to the text and/or graphics, which may alter content. The journal's standard [Terms & Conditions](#) and the [Ethical guidelines](#) still apply. In no event shall the Royal Society of Chemistry be held responsible for any errors or omissions in this *Accepted Manuscript* or any consequences arising from the use of any information it contains.

ARTICLE

Enhanced thermal conductivity for polyimide composites with a three-dimensional silicon carbide nanowires@graphene sheets filler

Cite this: DOI: 10.1039/x0xx00000x

Received 00th xxxx 201x
Accepted 00th xxxx 201x

DOI: 10.1039/x0xx00000x

www.rsc.org/

Wen Dai¹, Jinhong Yu^{1,2*}, Yi Wang¹, Yingze Song¹, Fakhr E Alam¹, Kazuhito Nishimura³, Cheng-Te Lin^{1*}, Nan Jiang^{1*}

Rigid three-dimensional structure composed of SiC nanowire@graphene sheets (3DSG) was prepared by high-frequency heating process. The polyamide acid was then infused into the three-dimensional structure and imidized at 350 °C. The thermal conductivity of PI/3DSG composites with 11 wt% filler addition can be up to 2.63 W/mK, approximately a ten-fold enhancement in comparison with that of neat PI. Furthermore, the 3DSG shows a better synergistic effect in thermal conductivity improvement, relative to simple mixture of SiC nanowires and GSs fillers with the same additive content. The reinforced thermal properties can be attributed to the formation of efficient heat conduction pathways among graphene sheets.

1. Introduction

Polyimide (PI) is widely used in microelectronics industries as for electronic packaging materials due to their light weight, high thermal and chemical stability, low dielectric constant and superior mechanical properties¹⁻³. However, the thermal conductivity of PI matrix is quite low, of the order of 0.1 W/mK at room temperature⁴, which cannot meet the heat-dissipating requirements of modern electronic and electrical systems. The poor thermal conductivity of PI is caused by the random orientation of the molecular chains in amorphous regions, which reduces the mean free path of heat conducting phonons. Efficient heat transfer and heat removal play a vital role for the long service life and high performance of electronic and photonic devices. Consequently, the fundamental studies of thermal conduction in advanced polymeric composites have been prompted. Recently, a variety of high thermally conductive nanomaterials has been adopted as efficient fillers to enhance the bulk thermal conductivity of PI⁵⁻⁷.

Graphene sheet (GS) is considered as the most promising filler to enhance the thermal conductivity of polymer matrix due to its high

intrinsic thermal conductivity (theoretical 5300 W/mK⁸), as well as the large specific surface area. Typical theory models indicate that heat conduction mechanism of polymer composites is due to the formation of heat conduction pathway within the matrix. When the concentration of filler reaches the percolation threshold (a critical value to form a continuous thermal conduction chain), the materials will possess excellent thermal conductivity to dissipate the heat generated. However, GSs usually tend to lie down flat in the polymer matrix when the concentration increases, as the result of the nature of its high aspect ratio⁹. This leads to difficulty in forming three-dimensional (3D) phonon conductive pathway, resulting in low thermal conductivity along through-plane direction. Therefore, the experimental value of thermal conductivity of graphene-based composites is far below the predicted value.

More recently, 3D interconnected graphene foam has gained much attention for application in various areas, especially as electrodes for high-performance batteries due to its excellent electrochemical capacities and an extremely large surface area with a low density¹⁰⁻¹³. Many efforts are made to synthesize 3D graphene by various techniques^{14, 15}. 3D Ni foam was in common used as template to grow graphene in CVD methods¹⁶⁻¹⁸. In a similar template method, the graphene solution was infused into the polymer foams and then the foams were etched to leave the 3D carbon skeleton. Obvious, this preparation on 3D graphene via template method is complex, expensive and time-consuming. On the other hand, the assembling of graphene by using freeze-drying technology is also another common approach¹⁹⁻²¹. The one-dimensional (1D) materials are often employed to uphold the original fragile 3D structure²². However, the interaction forces between the graphene and 1D material is the physical absorption which severely hampers the transfer of phonon

¹Key Laboratory of Marine Materials and Related Technologies, Zhejiang Key Laboratory of Marine Materials and Protective Technologies, Ningbo Institute of Materials Technology and Engineering, Chinese Academy of Sciences, Ningbo, 315201, China, E-mail: yujinhong@nimte.ac.cn, linzhengde@nimte.ac.cn, jiangnan@nimte.ac.cn

²Key Laboratory of New Processing Technology for Nonferrous Metals and Materials, Ministry of Education, School of Material Science and Engineering, Guilin University of Technology, Guilin 541004, China.

³Advanced Nano-processing Engineering Lab, Mechanical Systems Engineering, Kogakuin University, Kochi, 780-0805, Japan.

during the heat transfer. In addition, the freeze-drying method is also time-consuming. Currently, research on 3D graphene nanostructure fillers into polymer matrix is mainly focused on their mechanical and electrical properties^{11, 23-25}. The efforts on the high thermal transport from 3D graphene nanostructure have not attracted enough attention up to date.

In this study, we report a rapid and simple strategy for the preparation of 3D graphene nanostructure. The GSs were mixed uniformly with the Si and SiO₂ powder. Three dimensional structure SiC nanowires@graphene sheets (3DSG) were obtained by employing the high-frequency heating to process the mixed powder at high temperature. Subsequently, the 3DSG fillers were poured into the polymer matrix to enhance its thermal conductivity. In addition, in order to understand the synergistic effect of 3DSG fillers, the control groups with the same filler loading which were adopted the SiC nanowires, GSs and combined SiC-GSs fillers as filler were prepared. The thermal conductive properties of the PI/3DSG composites and its control groups were systematically investigated. The results demonstrated that the 3DSG fillers can effectively enhance the thermal conductivity of the polymer composite due to the formation of 3D interconnected network structure with significantly reduced thermal interface resistances.

2. Experimental

2.1. Materials

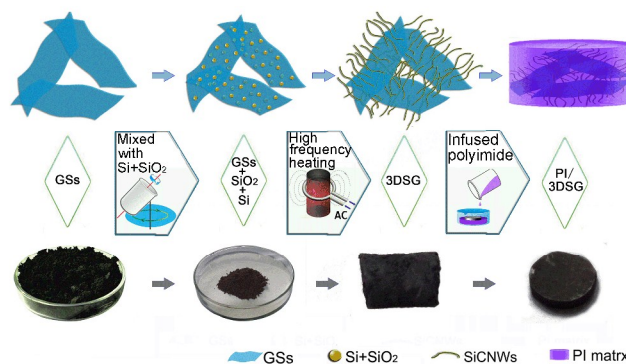
Commercial GSs were produced by Ningbo Institute of Materials Technology and Engineering (China). SiC nanowires grown through CVD method with a diameter of 100-600 nm and length 100 μm originate from Changsha Sinet Advanced Materials Co., Ltd (the characterization of SiC nanowires and GSs are shown in Supporting Information **Figure S1**). The silicon powder with average size of 1 μm and a purity of > 99.9% was supplied by Shanghai ST-Nano Science and Technology Co., LTD (China). The silica powder (0.2 μm) was purchased from Evonik Degussa (Germany). Poly(amic acid) (PAA) synthesized by pyromellitic dianhydride (PMDA) and 4,4-oxidianiline (ODA) were purchased from Ningbo Cen Electrical Material Co., Ltd (China). N,N'-dimethylacetamide (DMAc) were purchased Sinopharm Chemical Reagent co., Ltd (China) and used without further purification.

2.2. Preparation of 3DSG by high-frequency heating.

For the 3DSG hybrid sample preparation, 0.2 g GSs, 0.12 g Si and 0.25 g SiO₂ (the mole ratio is approximately 4:1:1, and the mole of Si was more than that of SiO₂ to guarantee the SiO₂ used up in next heating process) were mixed by using SpeedMixer. Then, the mixture powders were set into a graphite crucible and placed in the high frequency heating furnace in air to heat from room temperature to 1500 $^{\circ}\text{C}$ in several seconds. The heating time was kept for 8 min so that the unreacted SiO vapour diffused into the air. The growth mechanism for synthesizing the 3DSG was shown in **Figure S2**.

2.3. Preparation of PI/3DSG composites.

Firstly, the PAA was dissolved in DMAc at room temperature and the PAA solution was infused into the 3DSG along with vacuum degassing. Then, the as-prepared sample was



Scheme 1. Preparation process of the PI/3DSG composites.

cured moulding by thermally imidization in a vacuum oven at 80 $^{\circ}\text{C}$ for 2 h and 120, 150, 200, 250, 300, 350 $^{\circ}\text{C}$ for 1 h, respectively. The schematic drawing of experiment process are shown in **Scheme 1**. The 3DSG loading is 11 wt% consisted of GSs and SiC nanowires by thermogravimetry (**Figure S3**). For comparison purposes, the control group which were adopted 11 wt% SiC nanowires, 11 wt% GSs and 11 wt% SiC+GSs ($W_{\text{SiC}}:W_{\text{GSs}}=28:72$) as filler were prepared by solution blending and followed by the same thermally imidization as the preparation of PI/3DSG composites. The above three groups were denoted as PI/SiC, PI/GSs, and PI/SiC-GSs, respectively.

2.4. Characterization

The X-ray diffraction (XRD) patterns of the samples were recorded on a D8 DISCOVER With GADDS (BRUKER Ltd. Germany) with CuK α radiation ($\lambda=1.5406 \text{ \AA}$). The scanning was performed from 10 $^{\circ}$ to 80 $^{\circ}$ with a speed of 4 $^{\circ}\text{min}^{-1}$ at room temperature. The Raman spectra was recorded using a Reflex Raman System (RENISHAW plc, Wotton-under-Edge, UK) employing a laser wavelength of 532 nm. The photograph and microstructures of obtained samples were obtained by using camera (PENTAX K-30) and JEOL JEM-2100 (Japan Electron Optics Laboratory CO., Ltd, Japan) instrument with an acceleration voltage of 200 KV. The prepared powers were dispersed in ethanol by sonication for 15 min and some pieces were collected on 200 mesh carbon coated copper grids. The samples surface of the composites was examined on field emission scanning electron microscopy (FE-SEM, QUANTA FEG250, USA) at an acceleration voltage of 20 kV. Samples were broken and the fractured surface was coated with a thin layer of gold powder to avoid the accumulation of charge and improve conductivity. X-ray photoelectron spectroscopy (XPS) was carried out with a Kratos AXIS ULTR DLD spectrometer. Thermogravimetric analysis (TGA) was carried out with a Perkin-Elmer Pyris Diamond TG/DTA thermo-analyzer. The temperature range was from 30 to 900 $^{\circ}\text{C}$ at a heating rate of 3 $^{\circ}\text{C}/\text{min}$. Thermal conductivities of the composites were measured with LFA 457 Nanoflash apparatus (NETZSCH, Germany) at room temperature. The samples were prepared in round shape with the diameter of 6 mm and the thickness of 1 mm.

3. Result and discussion

3.1. Characterization of 3DSG

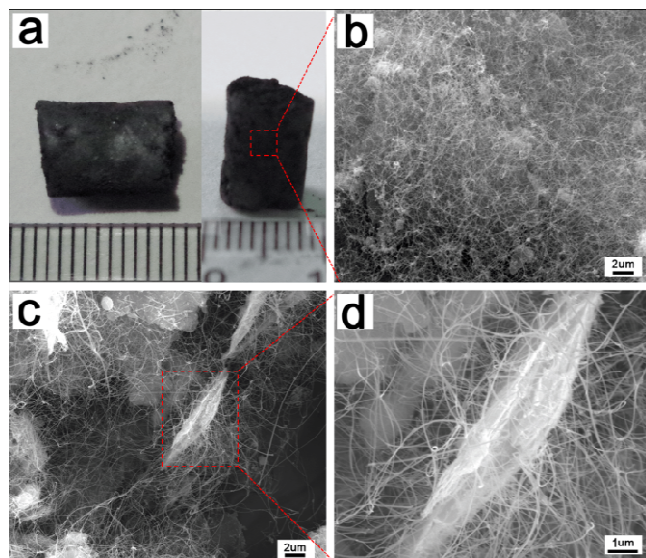


Figure 1. (a) Photographs of as-prepared 3DSG, (b) the surface SEM image of the 3DSG, (c) the inside SEM image of the 3DSG, and (d) an overview of individual GSs grown SiC nanowires.

In order to investigate the structure of as-prepared 3DSG, the macroscopic and microscopic morphology of the samples were shown in **Figure 1**. **Figure 1a** is the digital photo taken from the freestanding 3DSG showing that the 3DSG taken the shape of cylinder, with the diameter about 7 mm and height 10 mm. The density of 3DSG is 100-140 mg/cm³, which is much higher than that of other 3D graphene structure^{22, 26} due to its special synthetic method. **Figure 1(b-d)** shows the SEM images of the 3DSG with different investigated area. A rough and porous surface of the 3DSG from the **Figure 1a** was shown in **Figure 1b** and the SiC nanowires are clearly observable under low magnifications. The morphology and inside structure of the 3DSG is further observed to obtain more morphology details by high magnification SEM, as shown in **Figure 1c** and **Figure 1d**. It can be observed that the SiC nanowires are randomly distributed and loosely entangled as well as attached onto the GSs, thus forming a unique 3D structure. **Figure 1d** shows that the individual GSs with many SiC nanowires grown on GSs surface, demonstrating the typical component unit of the as-prepared 3DSG. It proved that the SiC nanowires possessed sufficient strength to assemble the GSs.

Figure 2a is the XRD pattern of the as-prepared 3DSG and its constituents are noted in the legend according to the JCPDS Card. The major diffraction peaks are present in **Figure 2a** are assigned to the (111), (200), (220), (311) and (222) reflections of cubic SiC (JCPDS Card No.29-1129) except the diffraction peaks from the GSs. A weak peak located the shoulder of the peak (111) is obvious due to the stacking faults in the (111) plane²⁷. It's important to note that the Si characteristic peak also appears in the XRD pattern, which may derive from the unspent raw material. The typical Raman spectra taken from SiC nanowires on the surface of GSs at room temperature is shown in **Figure 2b**. Three peaks at around 1337, 1556 and 2685 cm⁻¹ are characteristics peaks of the GSs, respectively, which can be assigned to D-band, G-band and 2D-band of GSs characteristic peak. The lower

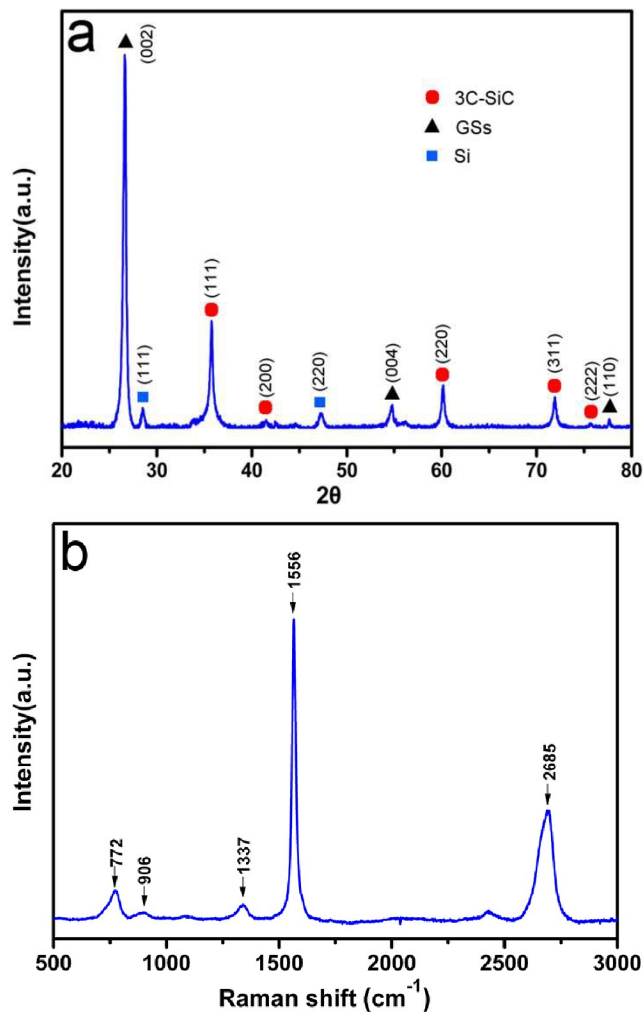


Figure 2. (a) XRD pattern and (b) Raman spectra of as-prepared 3DSG.

intensity ratio from the D-band to the G-band (I_D/I_G) demonstrates there is little defect of the GSs²⁸. In addition, the value, $I_{2D}/I_G = 0.57$, revealed that the GSs possess multilayered structure²⁹. The other two peaks at 772 and 906 cm⁻¹ in lower wavenumbers corresponds to absorption bands from transversal optic (TO) and longitudinal optic (LO) mode Si-C vibrations at the Γ point of cubic SiC³⁰ respectively, which suggests a single-crystalline 3C-SiC structure of the nanowires grown on the GSs surface. It can be noted that the peak at 772 and 906 cm⁻¹, respectively, showed a significant red shifts of 24 and 66 cm⁻¹ compared to the homologous phonon modes of bulk SiC³¹. The reason for this unique physical phenomena may derive from the confinement effect, inherent stacking faults and inner stress of the nanostructures^{32, 33}. Additionally, the broadening and asymmetry character of the Raman peak compared to that of bulk SiC could also be attributed to size confinement effects and the effect of stacking fault^{34, 35}. In contradiction to the XRD analysis, the Si characteristic peak nearby 520 cm⁻¹ is not appeared in the spectrogram. It suggests that the residual Si is negligible in the sample.

The TEM analysis provides clearer images of the microstructures of the as-prepared 3DSG, as shown in **Figure 3a**. The SiC nanowires were grown on the GSs surface, and the join (red arrow) could be

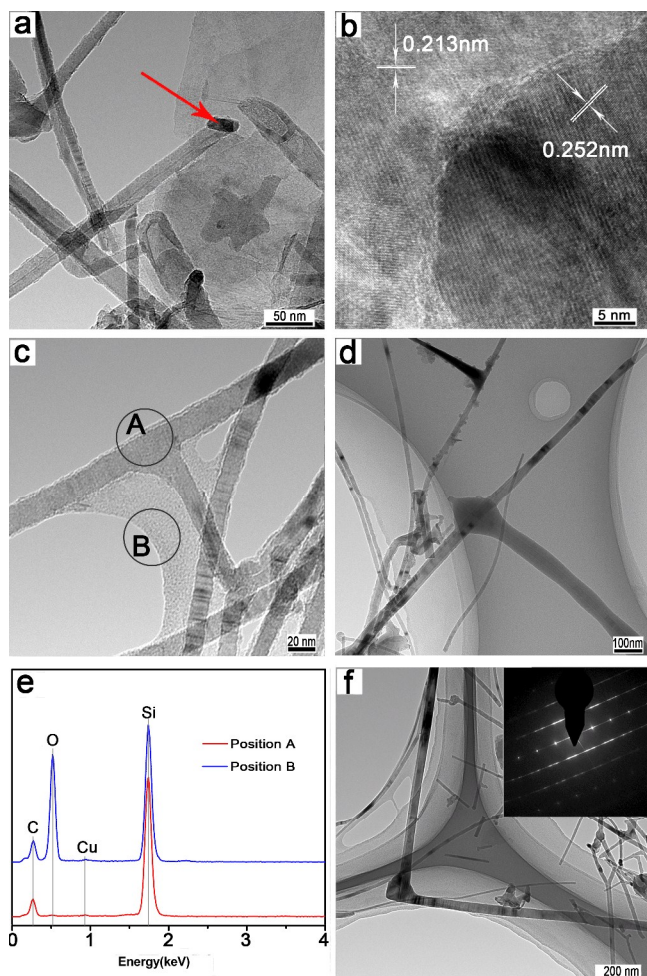


Figure 3. (a) The TEM image of the as-prepared 3DSG, (b) HRTEM image of red arrow region in (a), (c,d) the TEM image of the SiC nanowires, (e) the corresponding EDX spectrum in (c), and (f) representative TEM image of SiC nanowires and corresponding SEAD.

clearly seen in the **Figure 3a**. The matching together of two different lattices is observed in the HRTEM image of the join as shown in **Figure 3b**. The two atomic interplanar spacing annotated in the illustration is 0.213 and 0.252 nm. The former fits the hexagonal patterns from the honeycomb lattice of graphene³⁶. The latter is equal to the spacing of the (111) crystal faces of 3C-SiC (JCPDS Card No.29-1129). Additionally, the axis of the SiC nanowire is approximately parallel to the [111] direction, indicating that the SiC nanowire grows along the [111] direction. Notice from **Figure 3(c-d)** and **Figure 3f** that the SiC nanowire is associated with others rather than independent. The amorphous phase is the most common medium to connect the SiC nanowire as show in **Figure 3(c-d)**. The individual SiC nanowire touched with others, and the point of contact was packed by the amorphous phase. The EDX spectrum, as shown in **Figure 3e**, collected only from the nanowire (position A) shows that the nanowires contained C, Si, Cu and trace O, where the weak peak of Cu originates from the copper grid of TEM testing that is not the intrinsic signal of the nanowires. By comparison with the nanowires, there is a strong peak deemed as O appeared in the EDX spectrum taken from the amorphous phase (position B). Enormous quantities of oxide may come from the silicon oxide. **Figure 3f** showed the other way of connecting between the nanowires. It is not

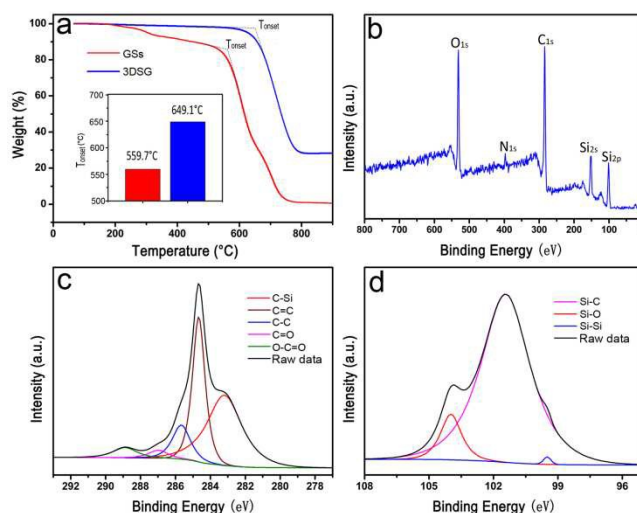


Figure 4. (a) TGA curves of GSs and 3DSG, (b) XPS survey spectra of as-prepared 3DSG, (c) the corresponding C1s XPS spectra, and (d) the corresponding Si2p XPS spectra.

several nanowires joined with each other but the sole nanowire grown bend and branch. The matching selected area electric diffraction patterns (SAED) inset in **Figure 3f** shows the 3C-SiC crystalline structure. The alignment of diffraction spots implies a high density of stacking fault, which is consistent with the above Raman spectrum (**Figure 2b**).

Figure 4a illustrates the typical TGA curves of the GSs and 3DSG in the air atmosphere. For GSs, as shown in the red curve in **Figure 4a**, there were two main weight loss steps for the GSs, one of which, at around 200-500 °C, was from the decomposition of oxygen-containing functional groups on the GSs, and the other, at around 500-800 °C, was from the thermal decomposition of the GSs structure. In contrast to GSs, where almost no significant weight loss for 3DSG is observed at 200-500 °C and only one weight loss steps present during the whole testing temperature. It's important to note that the onset temperature (T_{onset}) of the 3DSG is approximately 90 °C higher than that of the GSs, which may be ascribed to the anti-ablative performances of SiC. It suggests that 3DSG has good thermal stability. The residue weight of 3DSG is about 28 wt% after 800 °C as shown in the blue curve, which could be supposed to the nanowires. In order to further understand the atomic percentages and the group distribution, the 3DSG was analyzed by X-ray photoelectron spectroscopy (XPS). The XPS survey spectra of 3DSG was showed in **Figure 4b**, which exhibited five peaks assigned to C1s, O1s, N1s, Si2s and Si2p. The deconvolution of the C1s peaks was shown in the **Figure 4c**. It revealed peaks at 284.67, 283.19, 285.66, 286.97 and 288.89 eV correspond to C=C² (34.71%), C-Si³⁷ (46.29%), C-C (11.49%), C=O (2.92%), and O-C=O^{38, 39} (4.59%), respectively. The measured C-Si percentage is much higher than the TGA analysis due to the unevenly distributed of SiC nanowires. **Figure 4d** is the deconvolution of the Si2p peaks and it demonstrate the percentage of silicon containing compounds. The peaks at 101.43, 103.98 and 99.5 eV correspond to Si-C⁴⁰ (89.22%), Si-O (10.24%) and Si-Si⁴¹ (0.54%), respectively. The trace Si may stem from unspent Si powder, which is agreement with the XRD analysis.

3.2. The morphology of PI composites

To investigate the dispersion of fillers in the PI matrix, the fracture microstructure of neat PI and PI composites were observed by SEM shown in **Figure 5**. In the case of neat PI matrix, as shown in

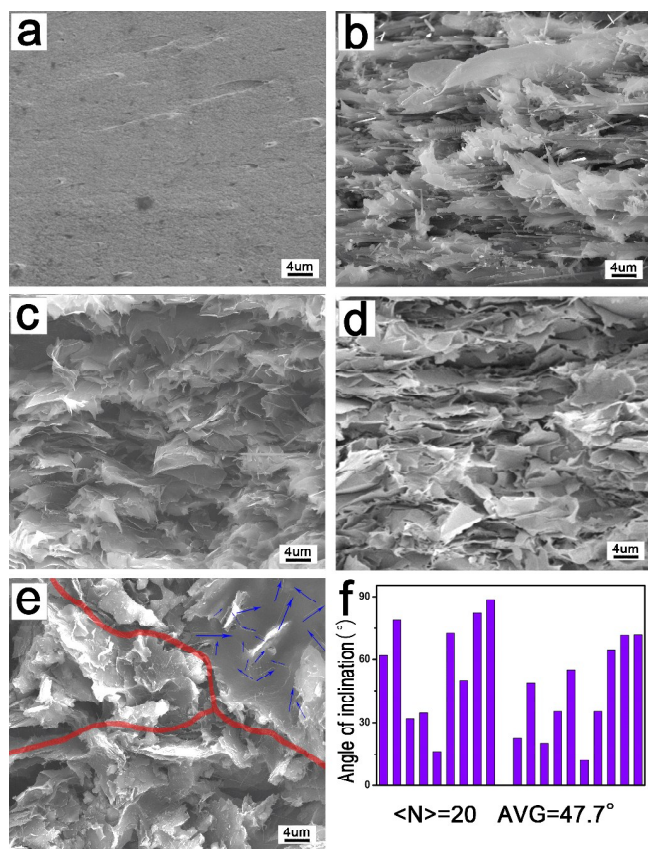


Figure 5. SEM images of fracture of: (a) neat PI, (b) PI/SiC, (c) PI/SiC-GSSs, (d) PI/GSSs, and (e) PI/3DSG, (f) histogram of measured value for SiC nanowire alignment in (e).

Figure 5a, the fracture surface of neat PI is homogeneous and smooth with only a few dots, which may be attributed to not be elastically relaxed after stretching out upon mechanical deformation. Compared to the neat PI, the morphology of the PI composites is rough and ridged due to the 1D or 2D geometry of filler (**Figure 5b-e**). The absence of aggregated SiC nanowires indicates that the nanowires were individually well dispersed with a sustained morphology within the PI matrix, as shown in **Figure 5b** and **5c**. Meanwhile, the pulled-out nanowires and the appearance of cracks were observed due to the poor binding interaction between the matrix and the filler. For the PI/GSSs composites, as shown in **Figure 5d**, the SEM micrographs of fracture surface also show well dispersion in the PI matrix and a sandwiched cross-sectional morphology consisting of GSSs. When a comparison is made between **Figure 5(b-d)** and **Figure 5e**, the filler, for 1D SiC nanowires or 2D GSSs, in the control group tends to lie down flat along the in-plane direction rather than random distribution that presented in the PI/3DSG composites. The acute angle between the horizontal and nanowires (blue arrows) of 20 pieces SiC nanowires in the part of the fracture surfaces are calculated and drawn into the histogram as shown in **Figure 5f**. The acute angle of SiC nanowires range from 0 to 85° with a mean angle is 47.7°, near to 45°, which show the randomness of the direction. It is noted that the dispersion of 3DSG in the PI matrix is not as good as the filler in the control group due to the 3D structure of the 3DSG. The PI acts as the basal body, and the GSSs join together into cross-linked network to form the carbon skeleton that is marked with red line in the **Figure 5e**.

3.3. Thermal conductivity of PI composites

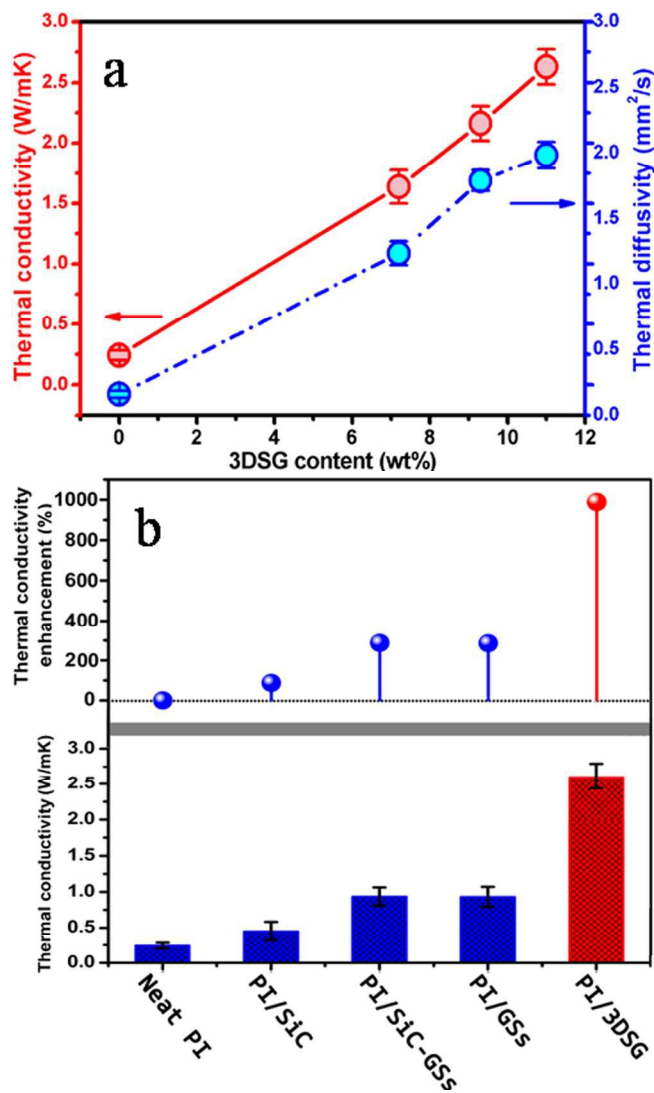


Figure 6. (a) Thermal conductivity and thermal diffusivity of PI/3DSG composites with various filler contents, (b) thermal conductivity and thermal conductivity enhancement of neat PI and PI composites.

The thermal conductivity and diffusivity of PI composites containing 3DSG fillers were examined as a function of the fillers content and the results are shown in **Figure 6a**. It is evident that the thermal conductivity increases monotonically with the incorporation of the 3DSG fillers. Similar to this, the curve of the thermal diffusivity of the composites also has a same trend. As can be seen, the thermal conductivity of PI composites with 0, 7.2, 9.3 and 11.0 wt% 3DSG fillers are 0.24, 1.64, 2.16 and 2.63 W/mK, respectively. In order to investigate the thermal conductivity improvement achieved by 3DSG fillers is remarkable compared with that achieved by SiC nanowires, GSSs, and combined SiC-GS fillers. **Figure 6b** presents the thermal conductivity and thermal conductivity enhancement of neat PI and PI composites with 11.0 wt% filler loading. The PI composites prepared with a 11.0 wt% loading of the individual fillers present thermal conductivities of 0.45 W/mK for the SiC nanowires filled composites and 0.93 W/mK for the GSSs filled composites. It was reported in previous literature that there is a synergistic effect to hybridize 1D-2D filler in improving the thermal conductivity⁴². Therefore, the

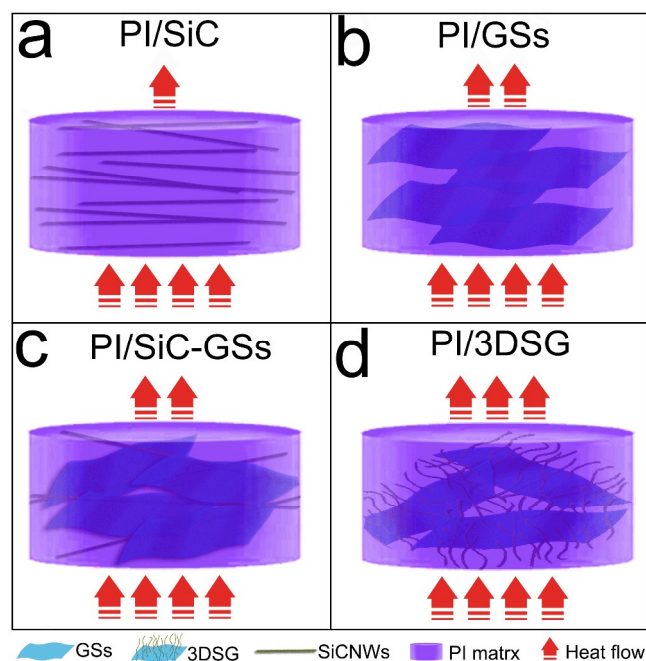


Figure 7. The model of heat flow for the composites: (a) PI/SiC, (b)PI/GSs, (c) PI/SiC-GSs, and (d) PI/3DSG.

extended experiments were carried out, with the purpose of investigating the synergistic effect of the SiC nanowires and GSs. As shown in **Figure 6b**, the thermal conductivity of PI composites with 11wt% SiC + GSs ($W_{\text{SiC}}:W_{\text{GSs}} = 28:72$) is 0.94 W/mK. The surprise is that the synergistic effect is negligible in this filler loading via solution blending method by comparing the thermal conductivity of PI/SiC, PI/GSs and PI/SiC-GSs. The synergism originates from the bridging of 2D nanosheets by the 1D nanowires. At 11.0 wt% loadings in this study, the 1D SiC nanowires and 2D GSs tend to lie down flat along the in-plane direction. The arrangements of GSs were not significantly different compared with the sole GSs filler in the same loading due to the steric hindrance, which dominates the contribution of the SiC nanowire bridges. However, in case of 3DSG fillers, the thermal conductivity of PI/3DSG composites was raised up to 2.63 W/mK, approximately a ten-fold enhancement compared with that of neat PI and a 182% enhancement compared with that of PI/SiC-GSs. The 3DSG filler demonstrates a strong synergistic effect and surpassed the thermal transport performance of the individual filler and hybrid 1D-2D filler. The remarkable synergistic behavior is attributed that the GSs join together into cross-linked network to form the heat conduction pathway and the direction of the nanowires are randomly dispersion, confirmed by **Figure 5e**. In comparison with the solution blending of SiC nanowires and GSs, the flat arrangements of the filler is substituted by random orientation with significantly increased of synergistic effect.

In order to explain the synergistic enhancement of the thermal conductivity of PI/3DSG composites, a model was proposed to present the efficient network for heat flow in the composites is shown in **Figure 7**. As shown in **Figure 7a**, heat flow of the PI/SiC composites is suppressed due to the presence of the polymer layer which separates the SiC nanowires in the network and precludes direct the SiC-SiC phonon transfer, which is agreement with the previous study for CNT embedded in polymer matrix^{43,44}. Even for a direct contact, the geometry of the junctions between two crossed SiC nanowires results in a point contact with extremely small contact area. Thus the interaction between nanowire and nanowire is very

Table 1 A comparison of various thermal conductive filler for polyimide composites.

Filler	Enhancement	Thermal Conductivity (W/mK)	Fraction	Reference
graphene	27 %	0.108	2.5 wt%	Koo, et al. ⁴⁵
graphene	294 %	1.002	11 wt%	Dai, et al. ⁹
GO	608 %	0.92	20 wt%	Tseng, et al. ³⁸
S-MWNTs	85 %	0.37	1.5 wt%	Tseng, et al. ⁴⁶
MgO	12 %	0.155	11.6 wt%	Murakami, et al. ⁴⁷
ZnO-NPs	410 %	1.54	59.1 wt%	Yorifuji, et al. ⁵
BN+AlN	500 %	1.2	30 wt%	Li, et al. ⁴
3DSG	989 %	2.63	11 wt%	This work

weak and the wrapping the polymer provides the dominant contributed to the heat flow. The broken heat flow along with SiC network is attributed to the involvement of the polymer matrix, as shown the green thermal conduction path in **Figure 7a**. The phonon mismatch between SiC nanowires and polymer matrix leads to a large thermal interface resistance. For PI/GSs composites, the GSs filler provides stronger enhancement of the thermal conductivity in comparison with SiC nanowires. The heat flow model of the PI/GSs composites is shown in **Figure 7b**, which presents the following factors: (1) the large surface aspect ratio of the GSs enhanced the GSs-polymer matrix interaction; (2) the unique 2D structure of GSs enhanced the contact area between GS and GS resulting in the thermal conduction path. On the other hand, the interruption of heat flow between GSs leads to a high thermal interface resistance and suppression of percolation. In the case of PI/SiC-GSs composites, as show in **Figure 7c**, the hybrid network does not provide synergistic enhancement to the thermal conductivity. This may be due to the following factors: (1) the weak Van der Waals forces attraction between SiC nanowires and GSs; (2) the presence of a thin layer of polymer prevents the direct contact between the SiC and GSs and acts as a scattering layer for the phonon transports. In contrast, the thermal conductivity of PI/3DSG achieved with the 3DSG filler was increased by approximately a factor of 3 when compared with the PI/SiC-GSs composites with the same loading. The 3DSG filler demonstrates a strong synergistic effect due to the 1D-SiC nanowire bridging adjacent 2D GSs in the 3D network and providing additional channels for the heat flow by passing the polymer matrix, as shown in **Figure 7d**. The model of heat flow for PI/3DSG composites shows the three phenomena as following: (1) the strong covalent bonding between SiC nanowires and GSs; (2) an interconnected network of 1D SiC nanowires providing fluent phonon transport path, confirmed by above TEM image; (3) the 3D structure leading to a decreased thermal resistance and considering as the major reason for the observed synergistic effect. Furthermore, the specific thermal conductivity value of PI/3DSG shows a ten-fold enhancement compared with that of neat PI from the values in **Figure 6**. The observed thermal conductivity of our study is comparable or much higher than various thermal conductive filler in the polyimide matrix in previous works^{4,5,9,38,45-47}. A comprehensive comparison is shown in **Table 1**.

4. CONCLUSION

In summary, we demonstrate a rapid and simple method to prepare 3DSG structure by high-frequency heating. The unique structure endows the high throughput transportation of phonon, resulting in excellent thermal conductive performances for PI composites. The thermal conductivity of PI/3DSG composites was raised up to 2.63 W/mK, approximately a ten-fold enhancement in comparison with that of neat PI. Furthermore, the 3DSG has a better synergistic effect in improving the thermal conductivity relative to the SiC nanowires

and GSs fillers with the same concentration by solution blending method. This new 3DSG hybrid filler is expected to be useful as novel and effective materials for thermal management application.

Acknowledgements

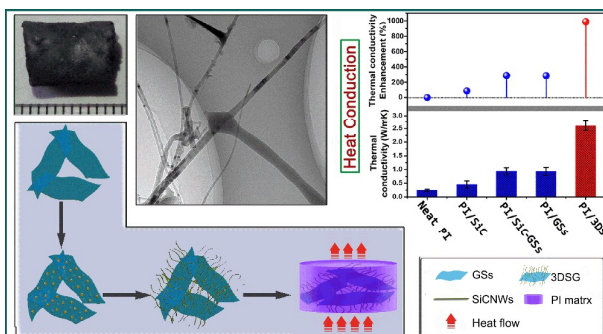
The authors are grateful for the financial support by the National Natural Science Foundation of China (51303034), Natural Science Foundation of Ningbo (Y40307DB05), Natural Science Foundation of Guangxi (2014GXNSFBA118034), and Guangxi Universities Scientific Research Project (YB2014165).

References

- J. Y. Wang, S. Y. Yang, Y. L. Huang, H. W. Tien, W. K. Chin and C. C. M. Ma, *J. Mater. Chem.*, 2011, **21**, 13569-13575.
- G. Y. Kim, M. C. Choi, D. Lee and C. S. Ha, *Macromol. Mater. Eng.*, 2012, **297**, 303-311.
- Z. Wu, D. Wu, W. Yang and R. Jin, *J. Mater. Chem.*, 2006, **16**, 310-316.
- T. L. Li and S. L. C. Hsu, *J. Phys. Chem. B*, 2010, **114**, 6825-6829.
- D. Yorifuji and S. Ando, *J. Mater. Chem.*, 2011, **21**, 4402-4407.
- M. Tanimoto, T. Yamagata, K. Miyata and S. Ando, *ACS Appl. Mater. Interfaces*, 2013, **5**, 4374-4382.
- Y. Zhang, S. Xiao, Q. Wang, S. Liu, Z. Qiao, Z. Chi, J. Xu and J. Economy, *J. Mater. Chem.*, 2011, **21**, 14563-14568.
- A. A. Balandin, S. Ghosh, W. Bao, I. Calizo, D. Teweldebrhan, F. Miao and C. N. Lau, *Nano Lett.*, 2008, **8**, 902-907.
- W. Dai, J. Yu, Y. Wang, Y. Song, H. Bai, K. Nishimura, H. Liao and N. Jiang, *Macromol. Res.*, 2014, **22**, 983-989.
- M. T. Pettes, H. Ji, R. S. Ruoff and L. Shi, *Nano Lett.*, 2012, **12**, 2959-2964.
- Z. Chen, W. Ren, L. Gao, B. Liu, S. Pei and H. M. Cheng, *Nature Mater.*, 2011, **10**, 424-428.
- H. Ji, L. Zhang, M. T. Pettes, H. Li, S. Chen, L. Shi, R. Piner and R. S. Ruoff, *Nano Lett.*, 2012, **12**, 2446-2451.
- J. Jia, X. Sun, X. Lin, X. Shen, Y. W. Mai and J. K. Kim, *ACS Nano*, 2014, **8**, 5774-5783.
- J. Liang, Y. Liu, L. Guo and L. Li, *RSC Adv.*, 2013, **3**, 11489-11492.
- D. A. Brownson, L. C. Figueiredo-Filho, X. Ji, M. Gómez-Mingot, J. Iniesta, O. Fatibello-Filho, D. K. Kampouris and C. E. Banks, *J. Mater. Chem. A*, 2013, **1**, 5962-5972.
- J. Chen, K. Sheng, P. Luo, C. Li and G. Shi, *Adv. Mater.*, 2012, **24**, 4569-4573.
- Y. H. Chang, C. T. Lin, T. Y. Chen, C. L. Hsu, Y. H. Lee, W. Zhang, K. H. Wei and L. J. Li, *Adv. Mater.*, 2013, **25**, 756-760.
- F. Luan, G. Wang, Y. Ling, X. Lu, H. Wang, Y. Tong, X. X. Liu and Y. Li, *Nanoscale*, 2013, **5**, 7984-7990.
- Y. Wei, S. Chen, D. Su, B. Sun, J. Zhu and G. Wang, *J. Mater. Chem. A*, 2014, **2**, 8103-8109.
- A. He, B. Lei, S. Li, L. Ma, S. Sun and C. Zhao, *RSC Adv.*, 2013, **3**, 22120-22129.
- Y. He, Y. Liu, T. Wu, J. Ma, X. Wang, Q. Gong, W. Kong, F. Xing, Y. Liu and J. Gao, *J. Hazard. Mater.*, 2013, **260**, 796-805.
- H. Sun, Z. Xu and C. Gao, *Adv. Mater.*, 2013, **25**, 2554-2560.
- C. Wu, L. Fang, X. Huang and P. Jiang, *ACS Appl. Mater. Interfaces*, 2014, **6**, 21026-21034.
- C. Wu, X. Huang, X. Wu, R. Qian and P. Jiang, *Adv. Mater.*, 2013, **25**, 5658-5662.
- C. Wu, X. Huang, G. Wang, L. Lv, G. Chen, G. Li and P. Jiang, *Adv. Funct. Mater.*, 2013, **23**, 506-513.
- M. A. Worsley, P. J. Pauzaskie, T. Y. Olson, J. Biener, J. H. Satcher Jr and T. F. Baumann, *J. Am. Chem. Soc.*, 2010, **132**, 14067-14069.
- J. Chen, Q. Shi and W. Tang, *Mater. Chem. Phys.*, 2011, **126**, 655-659.
- O. K. Park, J. Y. Hwang, M. Goh, J. H. Lee, B. C. Ku and N. H. You, *Macromolecules*, 2013, **46**, 3505-3511.
- A. Ferrari, J. Meyer, V. Scardaci, C. Casiraghi, M. Lazzeri, F. Mauri, S. Piscanec, D. Jiang, K. Novoselov and S. Roth, *Phys. Rev. Lett.*, 2006, **97**, 187401.
- M. Bechelany, A. Brioude, D. Cornu, G. Ferro and P. Miele, *Adv. Funct. Mater.*, 2007, **17**, 939-943.
- D. Olego and M. Cardona, *Phys. Rev. B*, 1982, **25**, 3889.
- S. I. Nakashima and H. Harima, *Phys. Status Solidi (a)*, 1997, **162**, 39-64.
- A. Meng, Z. Li, J. Zhang, L. Gao and H. Li, *J. Cryst. Growth*, 2007, **308**, 263-268.
- K. Senthil and K. Yong, *Mater. Chem. Phys.*, 2008, **112**, 88-93.
- Z. Li, J. Zhang, A. Meng and J. Guo, *J. Phys. Chem. B*, 2006, **110**, 22382-22386.
- G. Faggio, A. Capasso, G. Messina, S. Santangelo, T. Dikonimos, S. Gagliardi, R. Giorgi, V. Morandi, L. Ortolani and N. Lisi, *J. Phys. Chem. C*, 2013, **117**, 21569-21576.
- N. M. Bom, M. H. Oliveira Jr, G. V. Soares, C. Radtke, J. M. J. Lopes and H. Riechert, *Carbon*, 2014, **78**, 298-304.
- I. Tseng, J. C. Chang, S. L. Huang and M. H. Tsai, *Polym. Int.*, 2013, **62**, 827-835.
- L. B. Zhang, J. Q. Wang, H. G. Wang, Y. Xu, Z. F. Wang, Z. P. Li, Y. J. Mi and S. R. Yang, *Composites Part A*, 2012, **43**, 1537-1545.
- Q. B. Ma, J. Ziegler, B. Kaiser, D. Fertig, W. Calvet, E. Murugasen and W. Jaegermann, *Int. J. of Hydrogen Energy*, 2014, **39**, 1623-1629.
- J. Hu, Q. Lu, K. Tang, B. Deng, R. Jiang, Y. Qian, W. Yu, G. Zhou, X. Liu and J. Wu, *J. Phys. Chem. B*, 2000, **104**, 5251-5254.
- A. Yu, P. Ramesh, X. Sun, E. Bekyarova, M. E. Itkis and R. C. Haddon, *Adv. Mater.*, 2008, **20**, 4740-4744.
- N. Shenogina, S. Shenogin, L. Xue and P. Keblinski, *Appl. Phys. Lett.*, 2005, **87**, 133106.
- S. Shenogin, L. Xue, R. Ozisik, P. Keblinski and D. G. Cahill, *J. Appl. Phys.*, 2004, **95**, 8136-8144.
- M. Koo, J. S. Bae, S. E. Shim, D. Kim, D. G. Nam, J. W. Lee, G. W. Lee, J. H. Yeum and W. Oh, *Colloid Polym. Sci.*, 2011, **289**, 1503-1509.
- I. Tseng, H. C. Lin, M. H. Tsai and D. S. Chen, *J. Appl. Polym. Sci.*, 2012, **126**, 182-187.
- K. Murakami, K. Yamada, K. Deguchi, T. Shimizu and S. Ando, *J. Photopolym. Sci. Technol.*, 2010, **23**, 501-506.

Graphical Abstract

Table of contents entry:



Highlight:

3DSG incorporated into polyimide matrix greatly enhance its thermal conductivity (up to 2.63 W/mK), approximately a ten-fold enhancement in comparison with that of neat polyimide.